proteinase K (50 μg ml^{-1}) at 37 °C for 30 min and subjected to phenol–chloroform extraction, and RNA was recovered by ethanol precipitation. RNAs were separated by 10% PAGE and analysed by northern blotting with [α-^{32}P]GTP-labelled antisense U1, U2, U4, U5 and U6 snRNA probes[25].

Gel-shift assays

Gel-shift assays were done as described[17] except that β-globin RNA was used in the splicing assays. Recombinant His-tagged ASF/SF2, SRp38 and dSRp38 were prepared from recombinant baculovirus-infected Sf9 cells. ASF/SF2 (240 ng), pre-mRNA (16 ng), U1 snRNP (600 ng), dSRp38 (2–5 ng) and SRp38 (5 ng) was incubated under splicing conditions, except that ATP and creatine phosphate were omitted. Where indicated, dSRp38 or SRp38 was pre-incubated with U1 snRNP at 4 °C for 5 min, and reaction mixtures were incubated at 30 °C for 5 min. Heparin was then added to a concentration of 0.5 mg ml^{-1} and reaction mixtures were incubated at 30 °C for an additional 5 min. We loaded samples on 4% acrylamide:bisacrylamide (80:1) gels containing 50 mM Tris and 50 mM glycine, and electrophoresis was done at 14 V cm^{-1} for 3 h.

Details of western blotting, SRp38 depletion, splicing and generation of SRp38-deficient cells are given in the Supplementary Information.

Received 11 September; accepted 11 December 2003; doi:10.1038/nature02288.

1. Yost, H. J., Petersen, R. B. & Lindquist, S. RNA metabolism: strategies for regulation in the heat shock response. *Trends Genet.* **6,** 223–227 (1990).
2. Yost, H. J. & Lindquist, S. RNA splicing is interrupted by heat shock and is rescued by heat shock protein synthesis. *Cell* **45,** 185–193 (1986).
3. Bond, U. Heat shock but not other stress inducers leads to the disruption of a subset of snRNPs and inhibition of *in vitro* splicing in HeLa cells. *EMBO J.* **7,** 3509–3518 (1988).
4. Shukla, R. R., Dominiski, Z., Zwierzynski, T. & Kole, R. Inactivation of splicing factors in HeLa cells subjected to heat shock. *J. Biol. Chem.* **265,** 20377–20383 (1990).
5. Utans, U., Behrens, S. E., Luhrmann, R., Kole, R. & Kramer, A. A splicing factor that is inactivated during *in vivo* heat shock is functionally equivalent to the [U4/U6.U5] triple snRNP-specific proteins. *Genes Dev.* **6,** 631–641 (1992).
6. Gattoni, R. *et al.* The human hnRNP-M proteins: structure and relation with early heat shock-induced splicing arrest and chromosome mapping. *Nucleic Acids Res.* **24,** 2535–2542 (1996).
7. Mahe, D. *et al.* Cloning of human 2H9 heterogeneous nuclear ribonucleoproteins. Relation with splicing and early heat shock-induced splicing arrest. *J. Biol. Chem.* **272,** 1827–1836 (1997).
8. Bond, U. & James, T. C. Dynamic changes in small nuclear ribonucleoproteins of heat-stressed and thermotolerant HeLa cells. *Int. J. Biochem. Cell Biol.* **32,** 643–656 (2000).
9. Graveley, B. R. Sorting out the complexity of SR protein functions. *RNA* **6,** 1197–1211 (2000).
10. Manley, J. M. & Tacke, R. SR proteins and splicing control. *Genes Dev.* **10,** 1569–1579 (1996).
11. Shin, C. & Manley, J. L. The SR protein SRp38 represses splicing in M phase cells. *Cell* **111,** 407–417 (2002).
12. Arrigo, A. P. & Ahmad-Zadeh, C. Immunofluorescence localization of a small heat shock protein (Hsp23) in salivary gland cells of *Drosophila melanogaster*. *Mol. Gen. Genet.* **184,** 73–79 (1981).
13. Velazquez, J. M. & Lindquist, S. Hsp70: nuclear concentration during environmental stress and cytoplasmic storage during recovery. *Cell* **36,** 655–662 (1984).
14. Caputi, M., Mayeda, A., Krainer, A. R. & Zahler, A. M. hnRNP A/B proteins are required for inhibition of HIV-1 pre-mRNA splicing. *EMBO J.* **18,** 4060–4067 (1999).
15. Xiao, S. H. & Manley, J. L. Phosphorylation of the ASF/SF2 RS domain affects both protein–protein and protein–RNA interactions and is necessary for splicing. *Genes Dev.* **11,** 334–344 (1997).
16. Xiao, S. H. & Manley, J. L. Phosphorylation–dephosphorylation differentially affects activities of splicing factor ASF/SF2. *EMBO J.* **17,** 6359–6367 (1998).
17. Kohtz, J. D. Protein–protein interactions and 5′-splice-site recognition in mammalian mRNA precursors. *Nature* **368,** 119–124 (1994).
18. Wang, J., Takagaki, Y. & Manley, J. L. Targeted disruption of an essential vertebrate gene: ASF/SF2 is required for cell viability. *Genes Dev.* **10,** 2588–2589 (1996).
19. Wang, J., Xiao, S. H. & Manley, J. L. Genetic analysis of the SR protein ASF/SF2: interchangeability of RS domains and negative control of splicing. *Genes Dev.* **12,** 2222–2233 (1998).
20. Fukagawa, T., Regnier, V. & Ikemura, T. Creation and characterization of temperature-sensitive CENP-C mutants in vertebrate cells. *Nucleic Acids Res.* **29,** 3796–3803 (2001).
21. Nakai, A. & Ishikawa, T. Cell cycle transition under stress conditions controlled by vertebrate heat shock factors. *EMBO J.* **20,** 2885–2895 (2001).
22. Vogel, J. L., Parsell, D. A. & Lindquist, S. Heat-shock proteins Hsp104 and Hsp70 reactivate mRNA splicing after heat inactivation. *Curr. Biol.* **5,** 306–317 (1995).
23. Labourier, E. *et al.* Antagonism between RSF1 and SR proteins for both splice-site recognition *in vitro* and *Drosophila* development. *Genes Dev.* **13,** 740–753 (1999).
24. Dubois, M. F. *et al.* Heat shock of HeLa cells inactivates a nuclear protein phosphatase specific for dephosphorylation of C-terminal domain of RNA polymerase II. *Nucleic Acids Res.* **27,** 1338–1344 (1999).
25. Hall, K. B. & Konarska, M. M. The 5′ splice site consensus RNA oligonucleotide induces assembly of U2/U4/U5/U6 small nuclear ribonucleoprotein complexes. *Proc. Natl Acad. Sci. USA* **89,** 10969–10973 (1992).

Supplementary Information accompanies the paper on **www.nature.com/nature**.

Acknowledgements We thank Z. Chen, T. Kashima, S. Bush, Y. Shi and X. Li for plasmids and discussion; A. Norris and A. Doty for technical assistance; I. Boluk for help preparing the manuscript; R. Luhrmann and B. Kastner for purified U1 snRNP; and W. van Venrooij for antibodies against U1-70K. This work was supported by a grant from the NIH.

Competing interests statement The authors declare that they have no competing financial interests.

Correspondence and requests for materials should be addressed to J.L.M. (jlm2@columbia.edu).

Molecular engineering of a backwards-moving myosin motor

Georgios Tsiavaliaris[1,2], Setsuko Fujita-Becker[2] & Dietmar J. Manstein[1,2]

[1]*Institut für Biophysikalische Chemie, Medizinische Hochschule Hannover, OE 4350, Carl-Neuberg-Strasse 1, D-30623 Hannover, Germany*
[2]*Abteilung Biophysik, Max-Planck-Institut für Medizinische Forschung, Jahnstrasse 29, D-69120 Heidelberg, Germany*

All members of the diverse myosin superfamily have a highly conserved globular motor domain that contains the actin- and nucleotide-binding sites and produces force and movement[1,2]. The light-chain-binding domain connects the motor domain to a variety of functionally specialized tail domains and amplifies small structural changes in the motor domain through rotation of a lever arm[3,4]. Myosins move on polarized actin filaments either forwards to the barbed (+) or backwards to the pointed (−) end[5,6]. Here, we describe the engineering of an artificial backwards-moving myosin from three pre-existing molecular building blocks. These blocks are: a forward-moving class I myosin motor domain, a directional inverter formed by a four-helix bundle segment of human guanylate-binding protein-1 and an artificial lever arm formed by two α-actinin repeats. Our results prove that reverse-direction movement of myosins can be achieved simply by rotating the direction of the lever arm 180°.

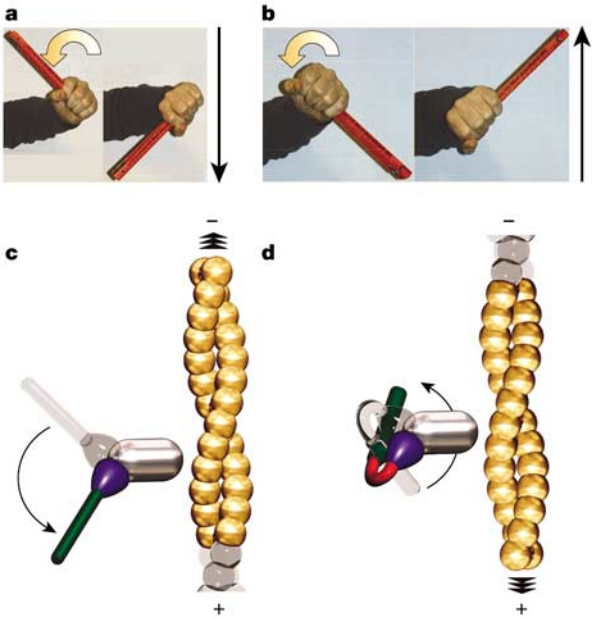

Figure 1 Mechanical models for myosin-based forwards and backwards movement. **a**, The translational movement of the tip of a lever (black arrow) depends on the angle of rotation and the direction in which the lever projects away from the axis of rotation. **b**, Simply by attaching the lever to the opposite site of the axis of rotation, the same rotation leads to a reversal of the translational movement of the lever. **c**, Power-stroke of a conventional barbed (+)-end-directed myosin. The converter region (blue) redirects the lever arm (green) such that it moves tangentially to the long axis of the actin filament (see also top views in Fig. 2). **d**, The insertion of an appropriately shaped domain (red) between the converter region and the lever arm reverses the direction of the power stroke and produces a pointed (−)-end-directed myosin. The myosin motor domain is shown in grey. The movement of the lever arm and force generation occur concomitantly with the release of ATP hydrolysis products. Additionally, myosin-based movement requires cyclic, ATP-dependent detachment and reattachment to actin filaments.

Most myosins move towards the barbed (+) end of actin filaments, but recent studies have established that at least one member of the family, myosin VI, moves towards the pointed (−) end[5]. The structural basis for reverse-direction movement has not been established. Two mechanisms for achieving reversal of myosin motility on the inherently polar actin filament have been suggested. On the basis of direct functional assays, electron microscopy and sequence analysis, Sweeney and co-workers proposed a model whereby reversal is achieved by rotating the lever arm in the opposite direction to conventional myosin lever arm movement[5] (Fig. 1). Ikebe and co-workers, however, measured the motile properties of chimaeric constructs and proposed that the core of the motor domain is the sole determinant of directionality[6].

To test whether rotating the lever arm 180° can itself produce reversal of directionality, we used molecular-engineering techniques. The constructs were based on the motor domain of the *Dictyostelium* class I myosin MyoE, which consists of 698 amino acids and will be referred to as E698. The structure of E698 is similar to that of conventional myosins[7], but it lacks an amino-terminal SH3-like subdomain. The absence of this subdomain prevents steric clashes between the motor domain and the engineered lever arm. Additionally, E698 produces a larger power stroke by moving the attached lever arm through a larger angle than the wild-type form does[7,8]. To rotate the lever arm in the opposite direction, we attached a four-helix bundle to the carboxy-terminal helix emerging from E698. The four-helix bundle comprises residues Leu 410 to Glu 508 of human guanylate-binding protein-1 (hGBP), the N-terminal tripeptide Arg-Glu-Met and a C-terminal Arg residue. The hGBP four-helix bundle, the structure of which has been determined to 1.8 Å resolution[9], is an ideal building block for achieving rotation of the lever arm. It is a highly rigid structure whose orientation, after fusion with the C-terminal helix of E698, can be accurately predicted. This fusion produces a forwards-stepping lever arm that is 4 nm in length and has the same orientation as the native LCBD (see Fig. 2).

A backwards-stepping lever arm 12 nm in length was created by the fusion of repeats 1 and 2 of α-actinin to the C-terminal helix of the hGBP four-helix bundle, which projects in the opposite direction to the helix emerging from the motor domain (see Supplementary movie 1). Previously, we have shown that the light-chain-binding domain (LCBD) of myosin II can be functionally replaced by building blocks consisting of two α-actinin repeats (2R) acting as an artificial lever arm[10–12]. We have also solved the structure of the *Dictyostelium* myosin II motor domain fused to 2R (ref. 13). Therefore, the structures of all the building blocks used for the generation of the backwards-moving motor E698-Ω2R are known, and they were connected by the direct fusion of α-helical regions of these building blocks. As a control, the motile activity of E698-Ω2R was compared to that of E698-2R, a barbed (+)-end-directed motor consisting of the MyoE motor domain fused to two α-actinin repeats. Models of E698-Ω2R and a myosin II motor domain fused to two α-actinin repeats (MD-2R) are shown in Fig. 2 bound to actin in the pre-power stroke state.

As the neck region of E698-Ω2R contains both forwards- and backwards-acting lever arm elements, the generation of force and movement by E698-Ω2R should depend on the motor's orientation during surface attachment. Unspecific attachment of E698-Ω2R to the surface is predicted to produce no movement or only short runs of back- and forth-moving actin filaments in the *in vitro* motility assay. Continuous movement of actin filaments requires specific attachment through either the backwards- or forwards-acting lever arm element to the surface of the assay compartment. Our results

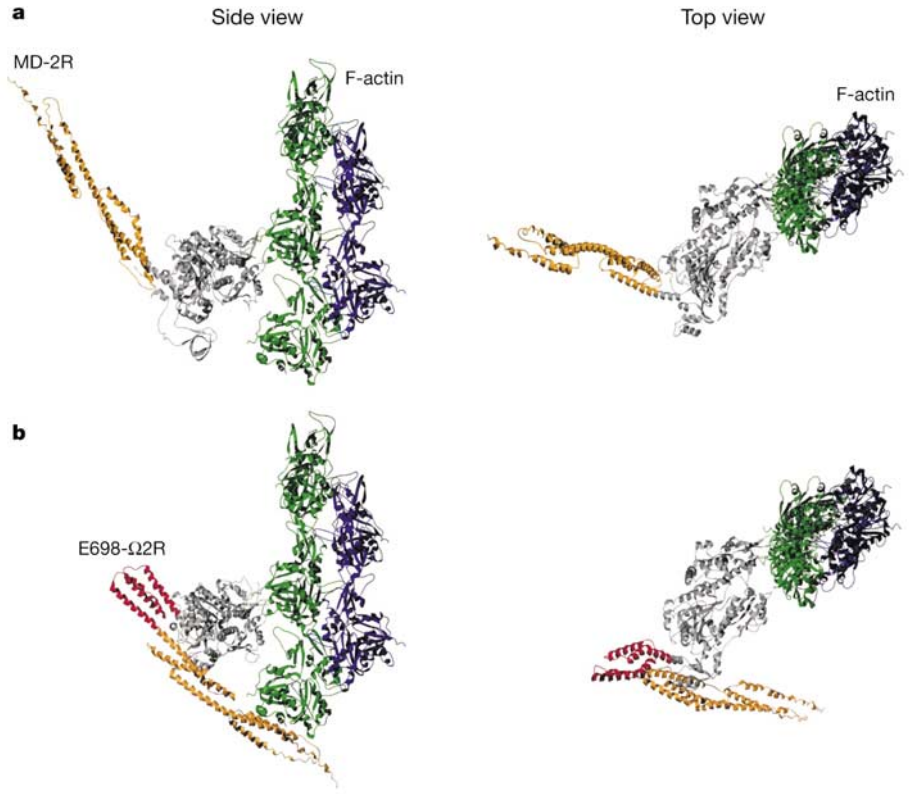

Figure 2 Molecular models of MD-2R and E698-Ω2R attached to F-actin. **a**, The artificial barbed (+)-end-directed motor MD-2R consists of a myosin II motor domain (grey) and an artificial lever arm formed by two α-actinin repeats (orange). **b**, The artificial pointed (−)-end-directed motor E698-Ω2R consists of the myosin I motor domain (grey), the hGBP four-helix bundle (red) and the lever arm (orange). The motors are modelled in the 'pre-power-stroke' state attached to an actin protofilament consisting of five actin monomers (green and blue).

show that these predictions are correct. Short runs of back- and forth-moving actin filaments were observed on surfaces decorated with unspecifically oriented E698-Ω2R (see Supplementary Fig. 1). The proportion of moving filaments decreased with increasing E698-Ω2R density on the surface owing to the resulting shortening in run length. By contrast, unspecifically attached E698-2R supported continuous sliding of actin filaments with a velocity of $0.62 \pm 0.01\,\mu m\,s^{-1}$ over a wide concentration range.

When the C-terminal His-tag, which is present in both E698-Ω2R and E698-2R, was used to attach the constructs in a specific orientation to the anti-His-tag antibody-coated surface, both constructs moved actin filaments continuously and with velocities of approximately $0.7\,\mu m\,s^{-1}$. Next, we determined the directionality of the motor constructs using polarity-marked actin filaments. Rhodamine/phalloidin was used to uniformly label and stabilize actin filaments, whereas Alexa Fluor 647 was used to label caps at the pointed (−) end. Rhodamine fluorescence is shown false-coloured in red and Alexa Fluor 647 fluorescence in green (Fig. 3a). Actin filaments moved with the pointed (−) end leading on surfaces that were coated either with E698-2R or with rabbit skeletal muscle heavy meromyosin (HMM). This result agrees with myosin-II-derived motors moving towards the barbed (+) end. By contrast, E698-Ω2R attached to an anti-His-tag antibody-coated surface moved filaments with the pointed (−) end trailing (Fig. 3a), indicating that E698-Ω2R is a pointed (−)-end-directed motor (see also Supplementary movies). The sliding velocities of labelled actin filaments obtained following their specific attachment are summarized in Fig. 3b. Positive velocity indicates movement towards the barbed (+) end, and negative velocity indicates movement towards the pointed (−) end of actin filaments. The wider distribution of velocities observed with E698-Ω2R results from a small but notable increase in the frequency of slow events. This bias is due to the presence of a small subpopulation of unspecifically attached E698-Ω2R in addition to antibody-bound E698-Ω2R.

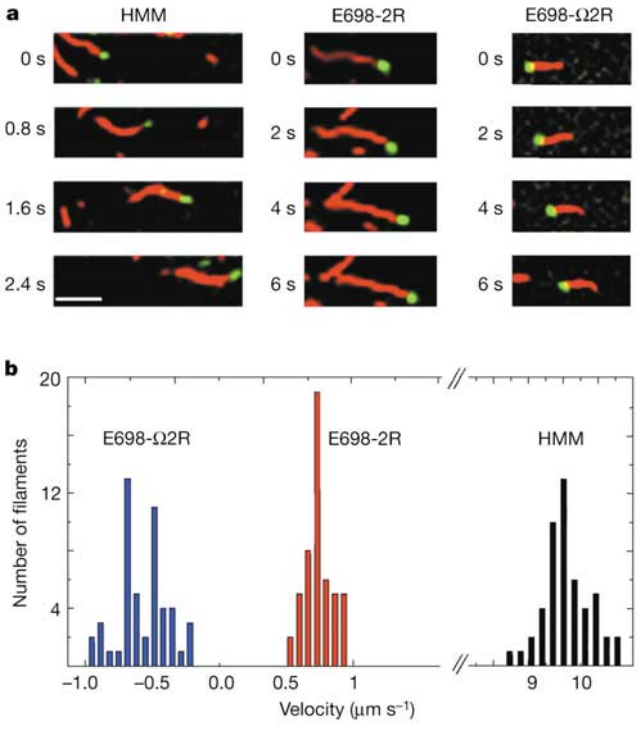

Figure 3 Direction of movement of myosin constructs. **a**, Movement of dual-labelled F-actin was visualized using a conventional *in vitro* motility assay[24]. The green tip marks the pointed (−) end. HMM and E698-2R move filaments with their green tips leading; E698-Ω2R moves them with their green tips trailing. Panels display the same spatial field at the relative times shown on the left. Bar, 10 μm. **b**, Histograms of the velocities of F-actin moving on surface-adsorbed HMM or on His-tag antibody-bound E698-2R and E698-Ω2R. Movement towards the barbed (+) end is defined as positive movement.

The results of the *in vitro* motility assays confirm the reversal of the directionality of a barbed (+)-end-directed motor. The similar absolute velocities of E698-Ω2R and E698-2R show that insertion of the hGBP four-helix bundle affects only the direction in which the lever arm projects away from the motor domain and not the protein's interactions with either nucleotides or actin. Our results agree with the findings of Sweeney and co-workers[5] on the directionality of myosin VI. They support a model that proposes that myosins and kinesins, both sharing a common fold consisting of seven β-strands and six α-helices[14,15], are intrinsically plus-end-directed motors. Conformational changes in the core motor domain are either amplified or amplified and redirected by the neck region in both protein classes. In evolutionary terms, the insertion of a small domain is a more favourable way to change motor direction than modification of the core motor domain and the basic mechanism by which the motor interacts with nucleotides and its filamentous protein track.

This work builds on protein-engineering approaches developed by our laboratory to elucidate the mechanism underlying motor protein action[16–22]. The control of critical motor parameters such as velocity, force and directionality should greatly facilitate future design and systematic characterization of novel motor proteins suitable for applications ranging from nano-technology to molecular medicine. The engineering of proteins with new and well-defined properties from known building blocks derived from biologically unrelated proteins has a wide range of applications. For example, we are combining fluorescent probe techniques with the engineered attachment of long amplifier elements to study the conformational dynamics of enzymes with high spatial and temporal resolution using near-field microscopy techniques. In addition, to change the dielectric properties of surfaces in a dynamic and tuneable manner, ordered arrays of molecular motors are being created on surfaces using molecular lithography and protein building blocks that support self-assembly into designed networks[23]. □

Methods

Protein engineering and purification

The expression vector for the production of E698-2R contains sequences encoding a translational fusion of the first 698 residues of *Dictyostelium* myosin IE, residues 264–505 of *Dictyostelium* α-actinin, eYFP and a C-terminal $(His)_8$ tag. The expression vector for the production of E698-2ΩR, in addition, contains the sequence encoding residues 410–508 of hGBP inserted between the myosin IE motor domain and the two α-actinin repeats. The mutation S336E was inserted into both constructs to mimic phosphorylation at the myosin TEDS site. For E698-2R, the sequence of the converter/2R fusion site reads LEMPRT/RASEQTK. For E698-Ω2R, the junction between the motor domain and four-helix bundle reads RTREM/LLQ and between the four-helix bundle and 2R it reads HER/RASEQTK. Expression and purification of the artificial motors from *Dictyostelium* were performed as described previously[16]. Rabbit HMM was prepared according to ref. 24, and rabbit skeletal muscle actin was purified as described previously[25].

Model building and figure preparation

The three-dimensional models of the myosin motor domains attached to F-actin in the 'pre-power-stroke' state were obtained by fitting the atomic models of F-actin[26], the myosin II motor domain construct MD-2R (ref. 27), and E698-Ω2R into the electron-density map of the *Dictyostelium* acto–S1 complex[28]. Model building was done with the program Swiss-PdbViewer[29]. Figures 1 and 2 were prepared using POV-Ray (Persistence of Vision Ray Tracer v3.02, 1997, http://www.povray.org).

Functional assays

Video-enhanced microscopy and analysis of actin filament sliding were performed as described previously[30]. Double labelling of F-actin was performed according to ref. 6 with minor modifications. G-actin was labelled with a 20-fold molar excess of Alexa Fluor 647 maleimide in the presence of 100 mM KCl, 5 mM $MgCl_2$, 1 mM EGTA and 25 mM imidazole-HCl, pH 7.5 (buffer A) in the dark for 2 h at 4 °C. The reaction was stopped by the addition of a two-fold excess of β-mercaptoethanol. The resulting actin filament seeds (0.5–2 μm in length) were collected by centrifugation (100,000 *g* for 10 min). Labelled filaments were separated from residual dye by gel filtration (Sephadex G-25) in 5 mM Tris, 0.2 mM $CaCl_2$, 1 mM NaN_3 at pH 7.5 (buffer B), and stabilized with phalloidin. For

elongation, a 10-fold molar excess of unlabelled G-actin in buffer B containing 100 mM KCl was added to the Alexa-Fluor-647-labelled filaments and the reaction was allowed to proceed for 30–120 min on ice. Finally, the double-labelled filaments were diluted to a final concentration of 5 to 20 nM, and the elongated part of the filaments was labelled and stabilized by the addition of rhodamine–phalloidin. Double-labelled filaments were only used fresh and were discarded after 12 h.

Received 3 September; accepted 19 December 2003; doi:10.1038/nature02303.

1. Toyoshima, Y. Y. *et al.* Myosin subfragment-1 is sufficient to move actin filaments *in vitro*. *Nature* **328,** 536–539 (1987).
2. Manstein, D. J., Ruppel, K. M. & Spudich, J. A. Expression and characterization of a functional myosin head fragment in *Dictyostelium discoideum*. *Science* **246,** 656–658 (1989).
3. Rayment, I. *et al.* Structure of the actin-myosin complex and its implications for muscle contraction. *Science* **261,** 58–65 (1993).
4. Berg, J. S., Powell, B. C. & Cheney, R. E. A millennial myosin census. *Mol. Biol. Cell* **12,** 780–794 (2001).
5. Wells, A. L. *et al.* Myosin VI is an actin-based motor that moves backwards. *Nature* **401,** 505–508 (1999).
6. Homma, K., Yoshimura, M., Saito, J., Ikebe, R. & Ikebe, M. The core of the motor domain determines the direction of myosin movement. *Nature* **412,** 831–834 (2001).
7. Kollmar, M., Dürrwang, U., Kliche, W., Manstein, D. J. & Kull, F. J. Crystal structure of the motor domain of a class-I myosin. *EMBO J.* **21,** 2517–2525 (2002).
8. Veigel, C. *et al.* The motor protein myosin-I produces its working stroke in two steps. *Nature* **398,** 530–533 (1999).
9. Prakash, B., Renault, L., Praefcke, G. J., Herrmann, C. & Wittinghofer, A. Triphosphate structure of guanylate-binding protein 1 and implications for nucleotide binding and GTPase mechanism. *EMBO J.* **19,** 4555–4564 (2000).
10. Uyeda, T. Q., Abramson, P. D. & Spudich, J. A. The neck region of the myosin motor domain acts as a lever arm to generate movement. *Proc. Natl Acad. Sci. USA* **93,** 4459–4464 (1996).
11. Anson, M., Geeves, M. A., Kurzawa, S. E. & Manstein, D. J. Myosin motors with artificial lever arms. *EMBO J.* **15,** 6069–6074 (1996).
12. Ruff, C., Furch, M., Brenner, B., Manstein, D. J. & Meyhöfer, E. Single-molecule tracking of myosins with genetically engineered amplifier domains. *Nature Struct. Biol.* **8,** 226–229 (2001).
13. Kliche, W., Fujita-Becker, S., Kollmar, M., Manstein, D. J. & Kull, F. J. Structure of a genetically engineered molecular motor. *EMBO J.* **20,** 40–46 (2001).
14. Kull, F. J. & Endow, S. A. Kinesin: switch I & II and the motor mechanism. *J. Cell Sci.* **115,** 15–23 (2002).
15. Vale, R. D. & Milligan, R. A. The way things move: looking under the hood of molecular motor proteins. *Science* **288,** 88–95 (2000).
16. Furch, M., Geeves, M. A. & Manstein, D. J. Modulation of actin affinity and actomyosin adenosine triphosphatase by charge changes in the myosin motor domain. *Biochemistry* **37,** 6317–6326 (1998).
17. Furch, M., Remmel, B., Geeves, M. A. & Manstein, D. J. Stabilization of the actomyosin complex by negative charges on myosin. *Biochemistry* **39,** 11602–11608 (2000).
18. Van Dijk, J. *et al.* Differences in the ionic interaction of actin with the motor domains of nonmuscle and muscle myosin II. *Eur. J. Biochem.* **260,** 672–683 (1999).
19. Knetsch, M. L. W., Uyeda, T. Q. & Manstein, D. J. Disturbed communication between actin- and nucleotide-binding sites in a myosin II with truncated 50/20-kDa junction. *J. Biol. Chem.* **274,** 20133–20138 (1999).
20. Tsiavaliaris, G. *et al.* Mutations in the relay loop region result in dominant-negative inhibition of myosin II function in *Dictyostelium*. *EMBO Rep.* **3,** 1099–1105 (2002).
21. Ponomarev, M. A., Furch, M., Levitsky, D. I. & Manstein, D. J. Charge changes in loop 2 affect the thermal unfolding of the myosin motor domain bound to F-actin. *Biochemistry* **39,** 4527–4532 (2000).
22. Reubold, T. F., Eschenburg, S., Becker, A., Kull, F. J. & Manstein, D. J. A structural model for actin-induced nucleotide release in myosin. *Nature Struct. Biol.* **10,** 826–830 (2003).
23. Ringler, P. & Schulz, G. E. Self-assembly of proteins into designed networks. *Science* **302,** 106–109 (2003).
24. Kron, S. J. & Spudich, J. A. Fluorescent actin filaments move on myosin fixed to a glass surface. *Proc. Natl Acad. Sci. USA* **83,** 6272–6276 (1986).
25. Lehrer, S. S. & Kerwar, G. Intrinsic fluorescence of actin. *Biochemistry* **11,** 1211–1217 (1972).
26. Lorenz, M., Poole, K. J., Popp, D., Rosenbaum, G. & Holmes, K. C. An atomic model of the unregulated thin filament obtained by X-ray fiber diffraction on oriented actin-tropomyosin gels. *J. Mol. Biol.* **246,** 108–119 (1995).
27. Dominguez, R., Freyzon, Y., Trybus, K. M. & Cohen, C. Crystal structure of a vertebrate smooth muscle myosin motor domain and its complex with the essential light chain: visualization of the pre-power stroke state. *Cell* **94,** 559–571 (1998).
28. Schröder, R. R. *et al.* Three-dimensional atomic model of F-actin decorated with *Dictyostelium* myosin S1. *Nature* **364,** 171–174 (1993).
29. Guex, N. & Peitsch, M. C. SWISS-MODEL and the Swiss-PdbViewer: an environment for comparative protein modeling. *Electrophoresis* **18,** 2714–2723 (1997).
30. Herm-Götz, A. *et al. Toxoplasma gondii* myosin A and its light chain: a fast, single-headed, plus-end-directed motor. *EMBO J.* **21,** 2149–2158 (2002).

Supplementary Information accompanies this paper on **www.nature.com/nature**.

Acknowledgements We thank S. Zimmermann for excellent technical assistance, R. Fedorov for providing Fig. 1, H. Faulstich for providing rhodaminephalloidin, C. Herrmann for the hGBP-1 cDNA, R. S. Goody, K. C. Holmes, M. A. Geeves, F. J. Kull, R. Maytum and D. P. Mulvihill for comments and discussions, and K. C. Holmes for continuous support. The work was supported by grants from the Deutsche Forschungsgemeinschaft (to D.J.M.).

Competing interests statement The authors declare that they have no competing financial interests.

Correspondence and requests for materials should be addressed to D.J.M. (manstein@bpc.mh-hannover.de).

Crystal structure and mechanism of a bacterial fluorinating enzyme

Changjiang Dong[1], Fanglu Huang[2], Hai Deng[1], Christoph Schaffrath[1], Jonathan B. Spencer[2], David O'Hagan[1] & James H. Naismith[1]

[1]*Centre for Biomolecular Sciences, The University of St Andrews, Fife KY16 9ST, UK*
[2]*University Chemical Laboratory, Lensfield Road, Cambridge CB2 1EW, UK*

Fluorine is the thirteenth most abundant element in the earth's crust, but fluoride concentrations in surface water are low and fluorinated metabolites are extremely rare[1,2]. The fluoride ion is a potent nucleophile in its desolvated state, but is tightly hydrated in water and effectively inert. Low availability and a lack of chemical reactivity have largely excluded fluoride from biochemistry: in particular, fluorine's high redox potential precludes the haloperoxidase-type mechanism[3,4] used in the metabolic incorporation of chloride and bromide ions. But fluorinated chemicals are growing in industrial importance, with applications in pharmaceuticals, agrochemicals and materials products[5–7]. Reactive fluorination reagents requiring specialist process technologies are needed in industry and, although biological catalysts for these processes are highly sought after, only one enzyme that can convert fluoride to organic fluorine has been described[8]. *Streptomyces cattleya* can form carbon–fluorine bonds[9] and must therefore have evolved an enzyme able to overcome the chemical challenges of using aqueous fluoride. Here we report the sequence and three-dimensional structure of the first native fluorination enzyme, 5′-fluoro-5′-deoxyadenosine synthase, from this organism. Both substrate and products have been observed bound to the enzyme, enabling us to propose a nucleophilic substitution mechanism for this biological fluorination reaction.

When grown in the presence of F^- ions, *S. cattleya* secretes fluoroacetate and 4-fluorothreonine, demonstrating its ability to biosynthesize organofluorine metabolites[9]. This organism contains an enzyme with a relative molecular mass (M_r) of 32,200 that has been shown to catalyse the formation of a C–F bond by combining *S*-adenosyl-L-methionine (SAM) and F^- to generate 5′-fluoro-5′-deoxyadenosine (5′-FDA) and L-methionine (ref. 10 and Fig. 1). Purification[11] and now overexpression of 5′-fluoro-5′-deoxyadenosine synthase (5′-FDAS) have allowed a fuller characterization of activity: the enzyme has a catalytic rate constant (k_{cat}) of

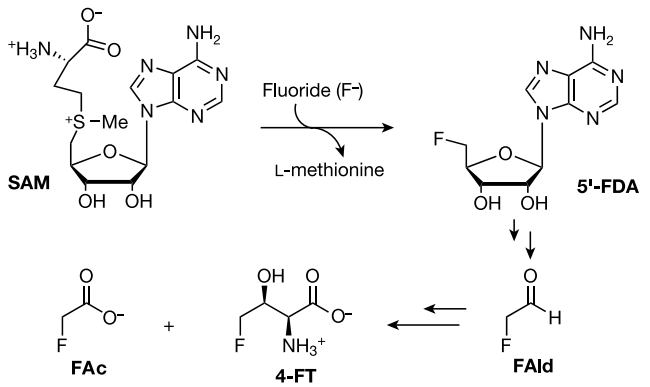

Figure 1 5′-FDAS from *S. cattleya* catalyses the formation of 5′-FDA from SAM and an F^- ion. 5′-FDA is the first-formed organofluorine metabolite, which is ultimately converted to fluoroacetate (FAc) and 4-fluorothreonine (4-FT) through fluoroacetaldehyde (FAld) by *S. cattleya*[30]. FAc is a toxin and 4-FT has antibiotic activity.